SLAC-PUB-6394
November 1993
(T/E)

ON THE APPLICABILITY OF FINITE ORDER PERTURBATIVE QCD CALCULATIONS OF JET RATES IN e^+e^- ANNIHILATION*

P.N. Burrows

Laboratory for Nuclear Science

Massachusetts Institute of Technology

Cambridge, MA 02139, USA

H. Masuda

Stanford Linear Accelerator Center

Stanford University, Stanford, CA 94309, USA

ABSTRACT

We have studied the measurement of α_s using exact second order QCD matrix element calculations of jet rates in $e^+e^- \rightarrow$ hadrons. We explain the dependence of $\alpha_s(M_Z^2)$, measured by experiments at the Z^0 resonance, on the choice of renormalisation scale in terms of the functional form of the three-jet matrix elements. We find that only a restricted domain of y_c, $\Lambda_{\overline{MS}}$, and scale gives a perturbation series which is well convergent, and that this domain is different for the various jet algorithms in current use. Small scales yield pathological perturbation series for any reasonable value of $\Lambda_{\overline{MS}}$.

* Work supported by Department of Energy contracts DE–AC02–76ER03069 (MIT) and DE–AC03–76SF00515 (SLAC).

1. Introduction

Quantum chromodynamics (QCD) is the accepted theory of strong interactions. Since it was first developed more than 20 years ago [1], QCD has been tested widely against data from many hard processes, and has been generally successful in explaining the features of the data [2], both qualitatively and quantitatively, up to the level of about 5–10% in accuracy. In many processes this accuracy is limited presently by the complexity of calculating observables to high order in perturbation theory, and in the non-perturbative regime.

In the case of e^+e^- annihilation, perturbative QCD calculations have been performed exactly up to third order in the strong coupling α_s for the hadronic cross-section ratio R [3] and the τ hadronic decay ratio R_τ [4]. However, observables related to the *structure* of hadronic events, such as jet rates [5] or thrust [6], have been calculated exactly only up to second order in perturbation theory [7,8]. These calculations have been used extensively by experiments at the PETRA, PEP, TRISTAN, SLC, and LEP colliders for extracting measurements of the strong coupling α_s [2].

One important consequence of truncating the perturbation series at low order is that there is a residual dependence on the QCD *renormalisation scale* μ. This parameter is formally unphysical and should not enter at all into an exact infinite order calculation. Within the context of a finite order calculation for a particular process the definition of μ depends on the renormalisation *scheme* employed,* and its value is in principle completely arbitrary. This *renormalisation scale ambiguity* has been discussed extensively, and several methods have been proposed which resolve the

* Here we consider calculations performed in the modified minimal subtraction scheme ($\overline{MS}$ scheme) [9].

ambiguity by choosing optimised scales according to different prescriptions [10,11,12]. These methods have not been without controversy [13,14]. Experimental groups have therefore adopted a pragmatic approach, usually avoiding the optimised scales, but taking into account the change in the QCD predictions when μ is varied across a range of values.

In Section 2 we summarise the experimental approach to α_s determination by fitting $O(\alpha_s^2)$ QCD predictions for hadronic event shapes in e^+e^- annihilation to data. We illustrate the complicated dependence of the fitted $\alpha_s(M_Z^2)$ values on the choice of renormalisation scale. In Section 3 we take jet rates as an example and review the form of the QCD calculations. We show, by comparing with recent data from the SLD collaboration, how this apparently complex $\alpha_s(M_Z^2)$ behaviour can be explained simply from the algebraic structure of the calculations. In Section 4 we study the range of applicability of the perturbative calculations of jet rates. Finally, in Section 5 we present a summary and concluding remarks.

2. The Experimental Approach

Consider the measurement of α_s by comparing $O(\alpha_s^2)$ calculations of event shape observables in $e^+e^- \rightarrow$ hadrons with data at the Z^0 resonance from SLC and LEP [2]. The experimental procedure is as follows: 1) the measured event shape distributions are corrected for detector bias effects such as acceptance, resolution, and inefficiency; 2) the data are further corrected for the effects of hadronisation using various models [15] to arrive at 'parton-level' distributions; 3) the perturbative QCD calculations are fitted to the data by varying the strong interaction scale $\Lambda_{\overline{MS}}$ * and minimising

* Unless stated otherwise, we always refer to $\Lambda_{\overline{MS}}$ for five active quark flavours.

χ^2, for fixed values of μ chosen within some *ad hoc* range;[1] 4) the resulting pairs of $\Lambda_{\overline{MS}}$,μ values are converted into $\alpha_s(M_Z^2)$ using the solution [16] of the renormalisation group equation; 5) for each observable a central value and *theoretical uncertainty* of $\alpha_s(M_Z^2)$ are quoted by taking the average and spread of the results in the chosen range of μ; 6) a grand average over the results from several observables is taken.

As a concrete example we show in Fig. 1 results from the SLD collaboration, taken from [17]. Values of $\alpha_s(M_Z^2)$ (Figs. 1(a) and (c)) and χ^2 per degree of freedom, χ^2_{dof}, (Figs. 1(b) and (d)) are shown from fits of $O(\alpha_s^2)$ QCD to SLD data in terms of jet rates (Section 3). The curves join values of $\alpha_s(M_Z^2)$ or χ^2_{dof} from fits to determine $\Lambda_{\overline{MS}}$ at discrete values of the renormalisation scale μ, plotted on the horizontal axis as $f = \mu^2/s$, where $\sqrt{s}$ is the centre-of-mass energy. The curve for each jet algorithm (Section 3) has the following qualitative characteristics:[2] 1) the fitted $\alpha_s(M_Z^2)$ depends strongly on the choice of f; 2) at high f, α_s increases monotonically and, for some algorithms, the fit quality worsens slightly as f is increased; 3) across a broad range of medium f the fit quality is reasonable and $\alpha_s(M_Z^2)$ changes slowly with f; 4) at lower f the fits are poor, χ^2_{dof} changes rapidly, and there is a pronounced maximum in α_s; 5) below this maximum small values of α_s are preferred, although the fit quality is very bad. Whilst the behaviour is qualitatively similar for each algorithm, numerically there are large differences between algorithms, with a tendency for the α_s values to diverge for $f \geq 0.1$. For example, at $f = 1$, $\alpha_s(M_Z^2)$ ranges from 0.109 (G algorithm) to 0.137 (E algorithm), a difference which is far larger than the (highly correlated) statistical errors on the measurements.

---

[1] Some experiments have also performed two-parameter fits by varying $\Lambda_{\overline{MS}}$ and μ simultaneously; these will be discussed in Section 4.

[2] As Figs. 1(c) and (d) are rather complicated, it may be instructive to look first at Figs. 1(a) and (b).

Such complicated behaviour is not restricted to α_s determined from jet rates. Similar figures for other event shapes, in addition to jet rates, may be found in Refs. [18] and [19]. This situation represents a serious problem for making accurate determinations of α_s by these techniques; not only is the fitted α_s highly correlated with the choice of renormalisation scale, but even at some arbitrarily chosen scale different observables yield values of α_s different from one another by more than the experimental errors. Here the experimentalists' pragmatic approach involves assigning to each observable an average $\alpha_s(M_Z^2)$, usually taken at the midpoint of the extrema of $\alpha_s(M_Z^2)$ in some chosen range of μ (see e.g. Figs. 1(a) and (c)), and a *scale uncertainty* representing the difference between the average value and the extrema. Only if the scale uncertainties are taken into account do the $\alpha_s(M_Z^2)$ values extracted from different observables agree within errors [19].

This procedure has been criticised [20], and it is certainly not unique. Each experiment has performed a similar analysis to extract α_s from event shapes, and each has adopted similar, but different, choices for the observables used, the range of μ, and the averaging method. This has naturally led to a variety of estimates of the theoretical uncertainty, which is larger than the experimental errors, and hence to apparent differences in overall precision on $\alpha_s(M_Z^2)$ measurements (Table 1). It is apparent that although some experiments may quote theoretical uncertainties as low as 6%, a sceptical observer [26] could be justified in concluding from the ensemble of results that the precision of these α_s determinations is realistically no better than about 10%.

In summary, results similar to Fig. 1 have been presented for a spectrum of event shapes used to determine α_s in e^+e^- annihilation. The behaviour of $\alpha_s(M_Z^2)$ and χ^2_{dof} as the renormalisation scale μ is varied is non-trivial and leads to large theoretical

Table 1. $\alpha_s(M_Z^2)$ and errors from $O(\alpha_s^2)$ QCD fits to jet rates.

Experiment	Algorithms	$\alpha_s(M_Z^2)$	Errors		Reference
			Exp.	Theor.*	
SLD	D,E,E0,P,P0,G	0.118	± 0.004	± 0.010	[17]
ALEPH	E0	0.121	± 0.004	$^{+0.010}_{-0.014}$	[21]
DELPHI	E,E0,P	0.114	± 0.005	± 0.012	[22]
	E0	0.118	± 0.001	± 0.009	[18]
L3	E0	0.115	± 0.005	$^{+0.012}_{-0.010}$	[23]
OPAL	E,E0,P,P0	0.118	± 0.003	± 0.007	[24]
	D,E,E0,P	0.124	± 0.003	$^{+0.010}_{-0.008}$	[19]
	D	0.119	± 0.004	± 0.009	[25]

*The theoretical uncertainty includes a contribution from the modelling of hadronisation corrections; this is typically small compared with the scale uncertainty.

uncertainties which dominate the error on the measurement of $\alpha_s(M_Z^2)$. However, we are not aware of any detailed investigation of the form of the dependence of $\alpha_s(M_Z^2)$ on scale extracted from the data. In the next section we present such a study for the case of jet rates.

3. Study of the Measured $\alpha_s(M_Z^2)$ Dependence on Renormalisation Scale

3.1 $O(\alpha_s^2)$ Calculations of Jet Rates

Jet structure in hadronic events may be defined using iterative clustering algorithms in which a measure y_{ij}, such as invariant mass-squared/s, is calculated for all pairs of particles i and j, and the pair with the smallest y_{ij} is combined into a single 'particle'. This process is repeated until all pairs have y_{ij} exceeding a value y_c, and the jet multiplicity of the event is defined as the number of 'particles' remaining. Various recombination schemes and definitions of y_{ij} have been suggested [27]. We

have applied the 'E', 'E0', 'P' and 'P0' variations of the JADE algorithm [28] as well as the more recently proposed 'Durham' ('D') [29] and 'Geneva' ('G') [27] algorithms, all of which are collinear and infra-red safe. These jet algorithms may be applied to both experimental measurements of hadronic events and QCD calculations at the parton level. The n-jet rate $R_n(y_c)$ is then defined as the fraction of the total event sample classified as n-jet.

For the three- and four-jet rates, calculated up to $O(\alpha_s^2)$ in QCD, we have [8]

$$R_3^i(y_c, \Lambda_{\overline{MS}}, f) \simeq \overline{\alpha_s}(\Lambda_{\overline{MS}}, f) A^i(y_c) \; + \; \overline{\alpha_s}^2(\Lambda_{\overline{MS}}, f)(A^i(y_c) 2\pi b_0 \ln f \; + \; B^i(y_c)) \quad (1)$$

$$R_4^i(y_c, \Lambda_{\overline{MS}}, f) \simeq C^i(y_c) \overline{\alpha_s}^2(\Lambda_{\overline{MS}}, f), \quad (2)$$

where $\overline{\alpha_s} \equiv \alpha_s/2\pi$; $b_0 = 23/12\pi$ for five active quark flavours; $f \equiv \mu^2/s$; i = D, E, E0, P, P0, G, and $A^i(y_c)$ and $B^i(y_c)$ are parametrised in Ref. [27].* Throughout this paper we use $\overline{s} = M_Z$. To the same order in perturbation theory the two-jet rate may be derived from the unitarity constraint

$$R_2 \quad = \quad 1 - R_3 - R_4. \quad (3)$$

In practice α_s is determined experimentally by fitting to the distribution of the quantity [30]:

$$D_2(y_c) \; \equiv \; \{R_2(y_c) - R_2(y_c - \Delta y_c)\}/\Delta y_c \quad (4)$$

thereby avoiding point-to-point correlations between jet rates at different y_c values. D_2 is then calculated to $O(\alpha_s^2)$ in QCD via Eq. (3). This is only a good approximation

* The expressions on the right hand sides of Eqs. 1 and 2 are actually normalised to σ_0, the lowest order cross-section for $e^+e^- \rightarrow q\bar{q}$. Before comparing with experimental data the right hand side should be divided by the factor $(1+\overline{\alpha_s})$. In order to simplify the algebra and clarify the following discussion we have neglected this factor. It amounts to a correction of about 4% [2] to the calculation of R_3 and R_4 and is properly considered by the experimentalists when they perform their fits.

in the region of phase space where the $R_{\geq 5}$ are small, *i.e.* away from small values of y_c. Fits to the data are usually restricted to the range of y_c [17] for which the measured $R_4 < 1\%$. The upper y_c fit boundary can be chosen to be the kinematic limit for (massless) 3-jet production, $y_c = 0.33$. From now on we call this range $\Delta^i y_c$; it is in general different for different jet algorithms i.

We now investigate the position of the stationary points of $D_2(y_c \in \Delta y_c)$ with respect to variation of f. Given that R_4 is required to be smaller than 1%, it is clear from Eqs. (3) and (4) that we may do this by considering the stationary points of R_3. The values of f at these points, f_s^i, are the solutions of[1]

$$\frac{\partial R_3^i}{\partial L}(y_c, \Lambda_{\overline{MS}}, f) \;=\; A^i(y_c)\frac{\partial \overline{\alpha_s}}{\partial L} + 2\overline{\alpha_s}\frac{\partial \overline{\alpha_s}}{\partial L}\{B^i(y_c) + 2\pi b_0 A^i(y_c) L\} + \overline{\alpha_s}^2 2\pi b_0 A^i(y_c) \;=\; 0, \tag{5}$$

where $L \equiv \ln f$, and [16]

$$\frac{\partial \overline{\alpha_s}}{\partial L} \quad = \quad \mu^2 \frac{\partial \overline{\alpha_s}}{\partial \mu^2} \quad = \quad -2\pi(b_0 \overline{\alpha_s}^2 + 2\pi b_1 \overline{\alpha_s}^3 + \ldots), \tag{6}$$

Equation (5) can be solved numerically for $f_s^i(\Lambda_{\overline{MS}}, y_c)$. We consider first the Durham algorithm and show in Fig. 2(a) the value of $f_s^D(y_c)$ at $\Lambda_{\overline{MS}} = 200$ MeV. It can be seen that for $y_c \in \Delta^D y_c$, f_s^D depends only weakly on y_c: $10^{-2} < f_s^D < 3 \times 10^{-2}$. From Eqs. (3) and (4) we therefore expect D_2^D to have stationary points at similar values of f. By taking the second derivative of R_3^D with respect to L one can show that the stationary point is a maximum.

[1] f_s^i coincides with the 'optimised' scale resulting from the 'PMS' prescription [12].

3.2 Comparison with Data

We show in Fig. 3 the calculations of $D_2^D(\Lambda_{\overline{MS}}, f)$ for y_c = (a) 0.03, (b) 0.10, and (c) 0.28, which span the range $\Delta^D y_c$ [17]. In each case the curves show $D_2^D(f)$ for six values of $\Lambda_{\overline{MS}}$ in the range $10 \leq \Lambda_{\overline{MS}} \leq 800$ MeV. Maxima in D_2^D are apparent at f close to the f_s^D shown in Fig. 2(a). Also shown as bands are the values of D_2^D *measured* by the SLD Collaboration [17]. The qualitative features are the same at each y_c. The calculations pass through the experimentally allowed region for $\Lambda_{\overline{MS}} \sim 200 \pm 150$ MeV. Within this region, at f values just above or below f_s^D *larger* values of $\Lambda_{\overline{MS}}$ are needed to fit the data. This gives rise to a *minimum* point in $\alpha_s(M_Z^2)$ at $f \sim f_s^D$ (Fig. 1(a)).

As f increases above f_s^D, successively larger $\Lambda_{\overline{MS}}$ values are needed to fit the data (Fig. 3). This translates into the monotonic rise in $\alpha_s(M_Z^2)$ for $f > 10^{-2}$ seen in Fig. 1(a). As f decreases below f_s^D the behaviour in Fig. 3 is rather complicated. For $10^{-3} < f < f_s^D$ larger $\Lambda_{\overline{MS}}$ values are needed to fit the data, but for $f < 10^{-3}$ the situation reverses; successively *smaller* $\Lambda_{\overline{MS}}$ values are required to make the calculation approach the data from below, but it always falls well short, even for $\Lambda_{\overline{MS}} \leq 10$ MeV. This explains the rise of $\alpha_s(M_Z^2)$ for $10^{-2} > f > 10^{-3}$ and the subsequent rapid falloff of $\alpha_s(M_Z^2)$ below $f \sim 10^{-3}$ (Fig. 1(a)), and the rapidly deteriorating fit quality for $f < 10^{-3}$ (Fig. 1(b)). The inability of the calculation to describe the data in this region is due to the fact that the next-to-leading term in R_3^D (Eq. (1)) is large and *negative* for $f < 10^{-3}$, and monotonically decreases as f decreases. The only way to compensate for this is to make $\Lambda_{\overline{MS}}$ very small. For a given $\Lambda_{\overline{MS}}$, R_3^D (and hence D_2^D) will ultimately become negative at sufficiently small scales (Fig. 3), which is an unphysical result.

We have repeated this study for the E, E0, P, P0 and G jet algorithms. For each case i, f_s^i, the calculated value of f at the stationary point of R_3^i, is shown in Fig. 2(b). The dependence of f_s^i on y_c is weak, except near the boundaries of phase space. For $y_c \in \Delta^i y_c$, comparison of f_s^i with f at the minimum of $\alpha_s(M_Z^2)$ versus f (Fig. 1(c)) shows good agreement. We have verified that, for each algorithm, the behaviour of $\alpha_s(M_Z^2)$ in Fig. 1(c) and χ^2_{dof} in Fig. 1(d) is explained in qualitatively the same fashion as for the D algorithm (Figs. 1(a) and (b)). The large χ^2_{dof} values at small scales (Figs. 1(b) and (d)) indicate that, in these domains, the $O(\alpha_s^2)$ calculations cannot be compared meaningfully with the data; this is due to the breakdown of the perturbative calculation of R_3. It is interesting to note that the upper f bound on these domains is algorithm-dependent.

4. Reliability of the Perturbative Approach

We now investigate more generally the reliability of the perturbative approach to the jet rates calculations. One expects a finite order perturbative calculation to provide a good approximation to the 'exact' answer if successive terms in the series decrease in magnitude as the order increases, *viz* if the perturbation series appears to be converging. In the present case only the first two terms of the series for R_3 are known. We define r as the ratio of the next-to-leading (NLO) to leading order (LO) contributions to R_3. In general r depends on y_c, $\Lambda_{\overline{MS}}$ and f. For given (y_c, $\Lambda_{\overline{MS}}$, f) the size of r gives an indication of the reliability of the calculation. If $|r| \gtrsim 1$, the perturbation series shows no sign of converging, so one has no reason to hope that the uncalculated higher order terms are small. Furthermore, if $r < -1$, $R_3 < 0$, which is unphysical. Equivalently, a given range of r defines a domain in (y_c, $\Lambda_{\overline{MS}}$, f) within which the calculation is convergent to the stated level.

In Fig. 4(a) we show $r(f)$ for the E, E0 and P algorithms and $\Lambda_{\overline{MS}} = 200$ MeV; in each case the band indicates the spread of $r(f)$ for $y_c \in \Delta y_c$. It can be seen that r increases monotonically with f, and that at a fixed scale the value of r is different for each algorithm. Results for the D, P0 and G algorithms are similar but are not shown for clarity. For either very large ($f \gg 1$) or very small ($f \ll 1$) scales the magnitude of r may not be small compared with unity, implying that perturbation theory cannot be reliably applied at such scales. In Fig. 4(b) we show the dependence [16] of α_s on f for the same value of $\Lambda_{\overline{MS}}$; for $f < 3 \times 10^{-5}$ the coupling constant exceeds unity.

In an attempt to quantify this discussion we choose ranges of r such that $|r| \leq \epsilon$ and calculate the corresponding ranges of $f(\Lambda_{\overline{MS}})$ for which this condition is satisfied for all $y_c \in \Delta y_c$. These ranges are shown in Fig. 5 for $\epsilon =$ (1) 0.0,* (2) 0.25, (3) 0.50 and (4) 1.0. A striking feature of Fig. 5 is that for a given condition, and at a chosen $\Lambda_{\overline{MS}}$ value, each algorithm has a different allowed range of f. For example, for $\epsilon = 0.25$ the allowed range for the E algorithm lies outside the allowed ranges for the other algorithms. Note also that $\epsilon < -1$ for $f \lesssim 10^{-5}$ with the E algorithm but for $f \lesssim 10^{-3}$ with the P algorithm. Great care must therefore be taken to use the $O(\alpha_s^2)$ calculation for a particular jet algorithm only within a sensible (y_c,$\Lambda_{\overline{MS}}$,f) domain. In particular, the E algorithm shows best convergence for small scales centred around $f \sim 10^{-4}$, but scales significantly smaller than $f \sim 10^{-3}$ yield pathological perturbation series for the other algorithms for any reasonable value of $\Lambda_{\overline{MS}}$.

Finally, in light of these obervations it is interesting to examine recent experimental determinations of $\alpha_s(M_Z^2)$ from measurements of jet rates at the Z^0 (Table 1). The SLD Collaboration used all six jet algorithms discussed here and

* The scale defined by this criterion corresponds with that resulting from the 'FAC' scale optimisation prescription [11]

found $\Lambda_{\overline{MS}} = 230 \pm 130$ MeV [17]. They quoted their results by considering measured values of $\alpha_s(M_Z^2)$ in the scale range $m_b^2/M_Z^2 < f < 4$ (see Fig. 1), where m_b is the b quark mass. This lower bound conveniently allows $\Lambda^{(5)}_{\overline{MS}}$ for five quark flavours to be used consistently throughout the analysis. From Fig. 5, the condition $|r| < 0.5$ is satisfied for the D, E0, P, P0 and G algorithms. For the E algorithm, however, $r > 0.5$ for most of their range of f.

The OPAL Collaboration has studied the E, E0, P and P0 algorithms [24,19], in addition to the D algorithm [19,25]. They estimated the scale uncertainty in their $\alpha_s(M_Z^2)$ measurement by considering $f_0 < f < 1$, where f_0 is the scale resulting from a simultaneous fit of both $\Lambda^{(5)}_{\overline{MS}}$ and f to their data, but in a range of y_c extended down to values such that the measured $R_5 \sim 1\%$. The upper limit on f is similar to the SLD choice, but the lower limit is not always the same. Their fitted $(\Lambda^{(5)}_{\overline{MS}}, f_0)$ values for the D, E0, P and P0 algorithms satisfy $|r| < 0.25$, but those for the E algorithm (111 MeV, 4×10^{-5}) [24] lie outside the $r < -0.5$ domain for y_c below 0.04, which is just outside their fit region. For $0.015 < y_c < 0.04$, $0.54 > R_4^E > 0.08$, *i.e.* R_4^E is sizeable relative to R_3^E, and has only been calculated at leading order. These large values of R_4^E explain the precipitous fall of the QCD calculation of D_2^E in the region $y_c < 0.03$ shown in Fig. 3 of Ref. [24]. Furthermore, in considering scales smaller than $f = m_b^2/s$ (m_c^2/s) one should probably use $\Lambda^{(4)}_{\overline{MS}}$ $(\Lambda^{(3)}_{\overline{MS}})$, the QCD interaction scale for 4 (3) active quark flavours, respectively, and then translate [16] the fitted values to $\Lambda^{(5)}_{\overline{MS}}$.

The L3 and DELPHI Collaborations studied the E0 algorithm within the scale range $10^{-3} \leq f \leq 1$ and found $70 \lesssim \Lambda^{(5)}_{\overline{MS}} \lesssim 370$ MeV [23,18], satisfying $|r| < 0.5$ (Fig. 5).

In summary, the $O(\alpha_s^2)$ QCD calculations of jet rates have been employed in domains of $(y_c, \Lambda_{\overline{MS}}, f)$ where the magnitude of the next-to-leading order contribution to the three-jet rate is typically not small, but is less than half the leading order contribution. The only exception is for calculations using the E algorithm, in which the relative contribution of the next-to-leading term is larger than 50% for $\Lambda_{\overline{MS}} > 150$ MeV and $f > 10^{-2}$, for example, a domain which has been included in $\alpha_s(M_Z^2)$ measurements presented by OPAL and SLD. The resulting $\alpha_s(M_Z^2)$ values have a stronger dependence on the renormalisation scale than those measured using the other jet algorithms.

5. Summary and Conclusions

We have studied the application of $O(\alpha_s^2)$ perturbative QCD calculations of jet rates in e^+e^- annihilation to the measurement of the strong coupling α_s. We have explained the non-trivial dependence of the measured values of $\alpha_s(M_Z^2)$ on the choice of renormalisation scale in terms of the structure of the calculations. Similar dependences have been presented [18,19] for other e^+e^- event shapes, and it is likely that their explanation is similar to the one we have described for jet rates.

We have studied the convergence properties of the $O(\alpha_s^2)$ perturbation series for the three-jet rate in terms of variation of the jet resolution parameter y_c, the renormalisation scale factor f, and the strong interaction scale $\Lambda_{\overline{MS}}$. We found that the magnitude of the next-to-leading contribution can be as large as (larger than) 50% of the leading contribution in some parts of the domains of $(y_c, \Lambda_{\overline{MS}}, f)$ used to measure α_s with the D, E0, P, P0, G (E) jet algorithms, respectively. The D, E0, P, P0 and G algorithms have pathological perturbation series for any reasonable value of $\Lambda_{\overline{MS}}$ at scales significantly smaller than $f \sim 10^{-3}$. Choosing the same range of f over

which to measure $\alpha_s(M_Z^2)$ for all algorithms can be dangerous, since the perturbation series does not necessarily show the same degree of convergence in each case.

Finally, we note that progress has recently been made in the form of 'resummed' QCD calculations of event shape distributions in e^+e^- annihilation [31]. So far, only the D algorithm has been found to have the necessary properties which allow the resummation technique to be used to calculate jet rates complete at leading, and partially at next-to-leading, order in $\ln(1/y_c)$, up to all orders in α_s [32]. The resulting all-orders calculation, valid in the region where $\alpha_s \ln(1/y_c) \leq 1$, may be combined with the fixed second order results discussed here to yield improved predictions for multi-jet rates at low y_c. Clearly similar caution must be exercised with these new procedures to ensure that the perturbative approach is reliable; this is discussed further in [17].

We thank our colleagues in the SLD experiment for support for this analysis. We also thank S. Bethke, S. Brodsky, Z. Kunszt, B. Lampe and B.R. Webber for helpful comments.

References

[1] H. Fritzsch, M. Gell-Mann, H. Leutwyler, Phys. Lett. **B47** (1973) 365.
D.J. Gross, F. Wilczek, Phys. Rev. Lett. **30** (1973) 1343.
H.D. Politzer, Phys. Rev. Lett. **30** (1973) 1346.

[2] For a review see S. Bethke, Proc. XXVI Int. Conf. on High Energy Physics, Dallas 1992, ed. J.R. Sanford, Vol. I, p. 81.

[3] S.G. Gorishny, A.L. Kataev, S.A. Larin, Phys. Lett. **B259** (1991) 144.
L.R. Surguladze, M.A. Samuel, Phys. Rev. Lett. **66** (1991) 560; *ibid* **66** (1991) 2416.

[4] E. Braaten, S. Narison, A. Pich, Nucl. Phys. **B373** (1992) 581.

[5] JADE Collab., S. Bethke *et al.* , Phys. Lett. **B213** (1988) 235.
TASSO Collab., W. Braunschweig *et al.*, Phys. Lett. **B214** (1988) 286.

[6] E. Farhi, Phys. Rev. Lett. **39** (1977) 1587.

[7] R.K. Ellis, D.A. Ross, A.E. Terrano, Phys. Rev. Lett. **45** (1980) 1226; Nucl. Phys. **B178** (1981) 421.
G. Kramer, B. Lampe, Z. Phys. **C39** (1988) 101; Fortschr. Phys. **37** (1989) 161.

[8] Z. Kunszt *et al.* , CERN 89–08 Vol I, (1989) p. 373.

[9] W.A. Bardeen, A.J. Buras, D.W. Duke, T. Muta, Phys. Rev. **18** (1978) 3998.
D.W. Duke, Rev. Mod. Phys. **52** (1980) 199.

[10] S.J. Brodsky, G.P. Lepage, P.B. Mackenzie, Phys. Rev. **D28** (1983) 228.

[11] G. Grunberg, Phys. Rev. **D29** (1984) 2315.

[12] P.M. Stevenson, Phys. Rev. **D23** (1981) 2916.

[13] H.J. Lu, S.J. Brodsky, U. of Md. PP # 93–087 (1993).

[14] P.M. Stevenson, DOE–ER–40717–2 (1993).

[15] For a review see: T. Sjöstrand *et al.* , CERN 89–08 Vol. 3, (1989) p. 143.

[16] K. Hikasa *et al.*, Phys. Rev. **D45** 11 (1992) III.54.

[17] SLD Collab., K. Abe *et al.* , Phys. Rev. Lett. **71** (1993) 2528.

[18] DELPHI Collab., P.Abreu *et al.* , Z. Phys. **C54** (1992) 55.

[19] OPAL Collab., P.D.Acton *et al.* , Z. Phys. **C55** (1992) 1.

[20] D.T. Barclay, C.J. Maxwell, DTP–92/26 (1992).

[21] ALEPH Collab., D.Decamp *et al.* , Phys. Lett. **B255** (1991) 623.

[22] DELPHI Collab., P.Abreu *et al.* , Phys. Lett. **B247** (1990) 167.

[23] L3 Collab., P.Adeva *et al.* , Phys. Lett. **B248** (1990) 464.

[24] OPAL Collab., M.Z. Akrawy *et al.* , Z. Phys. **C49** (1991) 375.

[25] OPAL Collab., P.D. Acton *et al.* , Z. Phys. **C59** (1993) 1.

[26] G. Altarelli, CERN–TH–6623–92 (1992).

[27] S. Bethke *et al.* , Nucl. Phys. **B370** (1992) 310.

[28] JADE Collab., W. Bartel *et al.*, Z. Phys. **C33** (1986) 23.

[29] N. Brown, W.J. Stirling, RAL–91–049 (1991).

[30] Mark II Collab., S. Komamiya *et al.* , Phys. Rev. Lett. **64** (1990) 987.

[31] S. Catani, L. Trentadue, G. Turnock, B.R. Webber, Nucl. Phys. **B407** (1993) 3.

[32] S. Catani *et al.* , Phys. Lett. **B269** (1991) 432.

Figure Captions

FIG. 1. (a) $\alpha_s(M_Z^2)$ and (b) χ^2_{dof} from $O(\alpha_s^2)$ QCD fits to jet rates in $Z^0 \to$ hadrons, calculated with the Durham algorithm (see text). The band indicates the size of statistical errors on the SLD measurements. (c), (d) are as (a), (b) for jet rates calculated according to the E, E0, P, P0 and G algorithms.

FIG. 2. The value of the renormalisation scale factor at the stationary point of R_3, $f_s(y_c)$, for the (a) D, (b) E, E0, P, P0 and G jet algorithms, and $\Lambda_{\overline{MS}} = 200$ MeV. The arrows indicate the range $\Delta^i y_c$ for each algorithm i (see text).

FIG. 3. $D_2(\Lambda_{\overline{MS}}, f)$ calculated with the Durham algorithm for $y_c =$ (a) 0.03, (b) 0.10, (c) 0.28. In each case six curves are shown for the values of $\Lambda_{\overline{MS}}$ indicated.

The shaded bands represent the value of D_2 measured by SLD, including the one standard deviation uncertainty.

FIG. 4. (a) The ratio $r(f)$ (see text) calculated for the E, E0 and P jet algorithms at $\Lambda_{\overline{MS}} = 200$ MeV. The bands indicate the range of r corresponding to $y_c \in \Delta^i y_c$ for each algorithm i. (b) $\alpha_s(f)$ for $\Lambda_{\overline{MS}} = 200$ MeV.

FIG. 5. The range of f within which $|r(\Lambda_{\overline{MS}}, f)| \leq \epsilon$ for the (a) D, (b) E, (c) E0, (d) P, (e) P0 and (f) G jet algorithms. In each case the curves mark the boundary of the f range for $\epsilon = 0$, 0.25, 0.5 and 1.0.

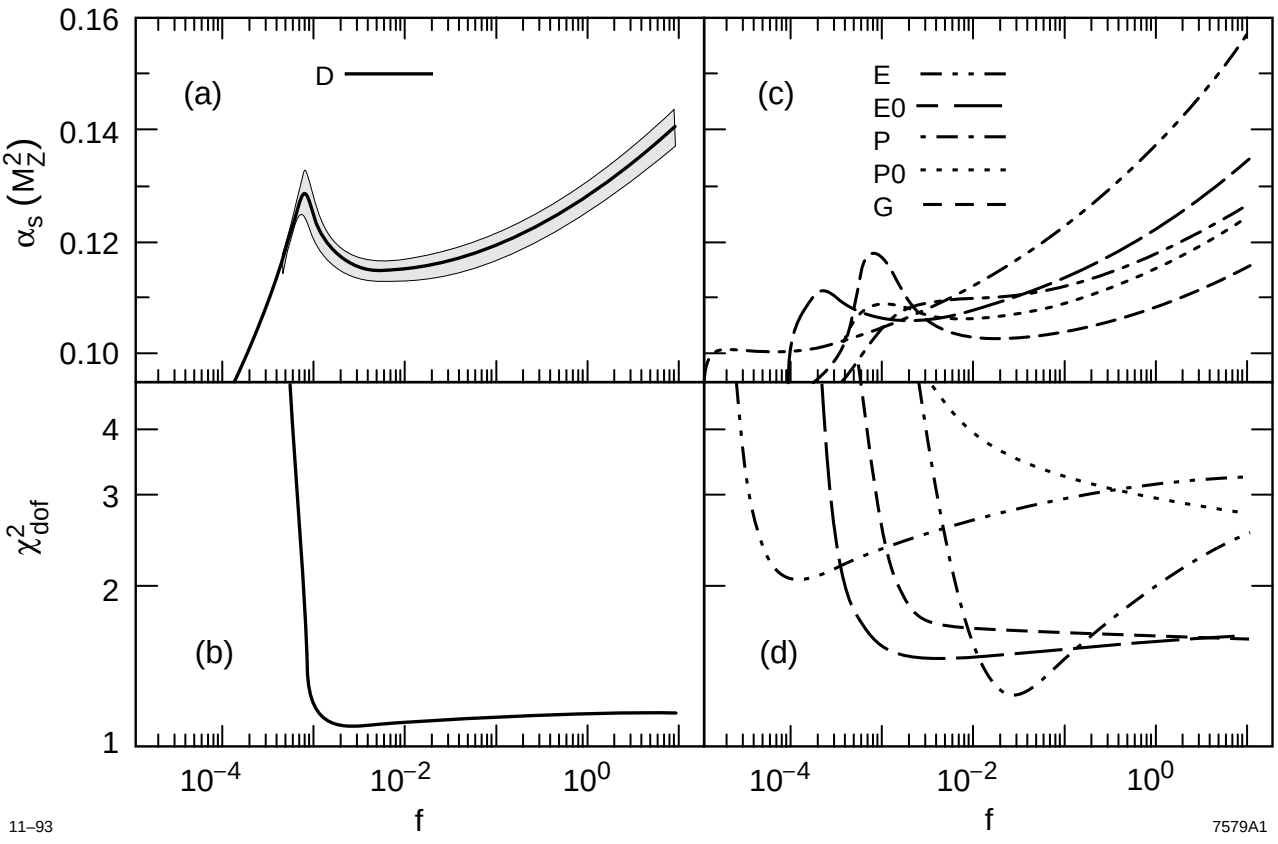
0.16
0.14
0.12
0.10
$\alpha_s(M_Z^2)$
(a)
D
(c)
E
E0
P
P0
G
4
3
2
1
χ^2_{dof}
(b)
(d)
10^{-4}
10^{-2}
10^{0}
f
11–93
7579A1

Fig. 1

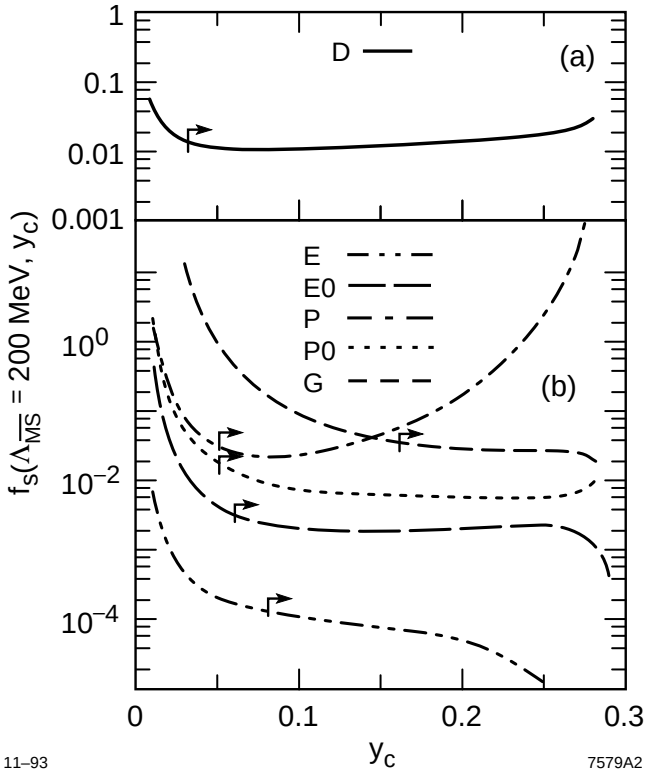
1
0.1
0.01
0.001
D
(a)
E
E0
P
P0
G
(b)
10^0
10^{-2}
10^{-4}
$f_S(\Lambda_{\overline{MS}} = 200\ MeV, y_c)$
0
0.1
0.2
0.3
y_c
11–93
7579A2

Fig. 2

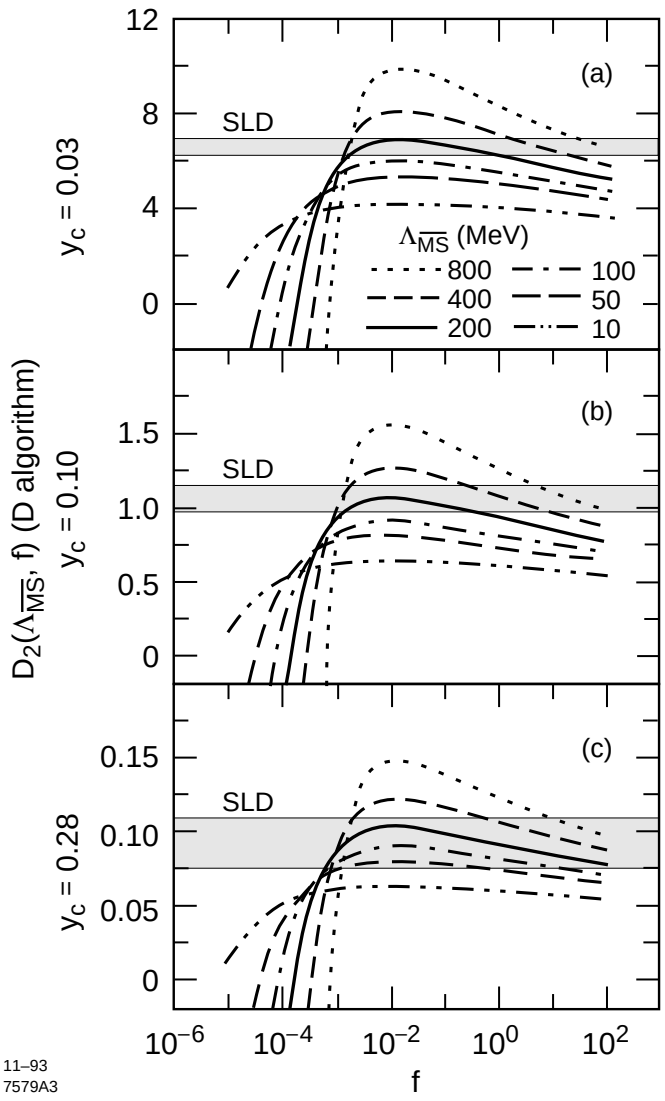
12
8
4
0
(a)
SLD
y_c = 0.03
$\Lambda_{\overline{MS}}$ (MeV)
800
400
200
100
50
10
1.5
1.0
0.5
0
(b)
SLD
y_c = 0.10
0.15
0.10
0.05
0
(c)
SLD
y_c = 0.28
$D_2(\Lambda_{\overline{MS}}, f)$ (D algorithm)
10^{-6}
10^{-4}
10^{-2}
10^{0}
10^{2}
f
11–93
7579A3

Fig. 3

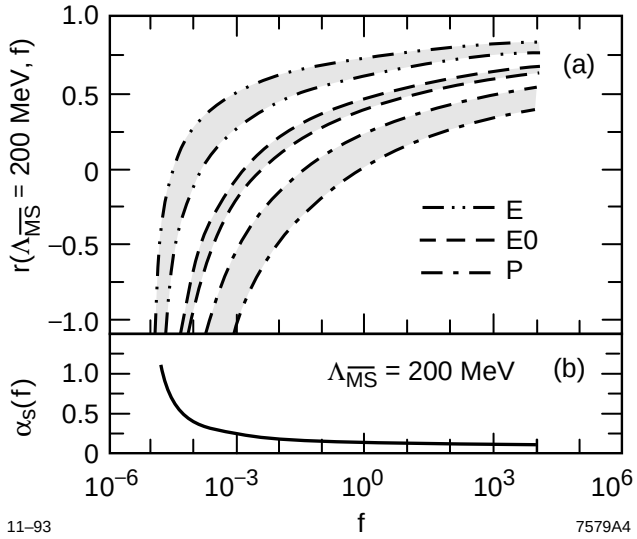
1.0
0.5
0
−0.5
−1.0
r(Λ$\overline{MS}$ = 200 MeV, f)
(a)
E
E0
P
Λ$\overline{MS}$ = 200 MeV
(b)
1.0
0.5
0
αs(f)
10−6
10−3
100
103
106
f
11–93
7579A4

Fig. 4

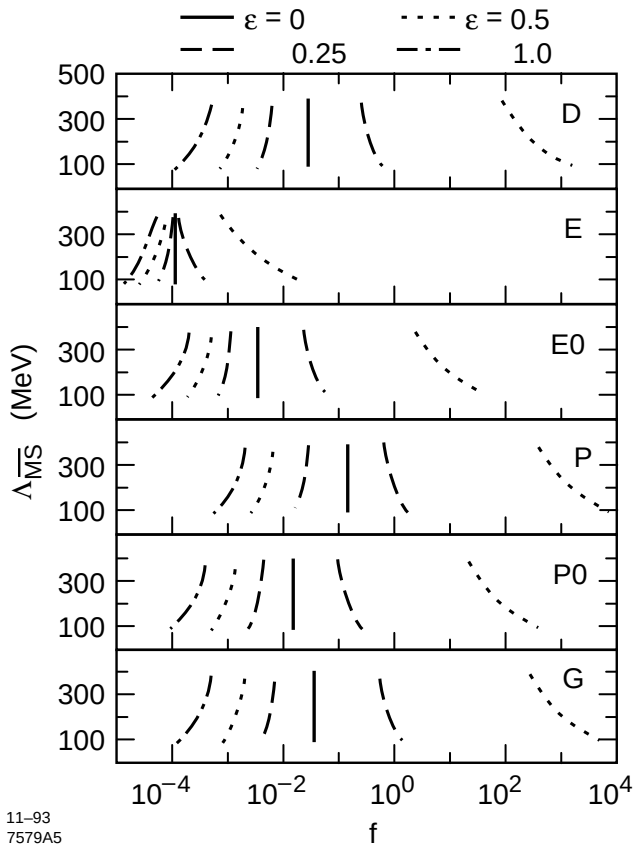
ε = 0
ε = 0.5
0.25
1.0
500
300
100
D
E
E0
P
P0
G
$\Lambda_{\overline{MS}}$ (MeV)
10^{-4}
10^{-2}
10^{0}
10^{2}
10^{4}
f
11–93
7579A5

Fig. 5